Astron. Astrophys. 356, 676–690 (2000)

ASTRONOMY AND ASTROPHYSICS

Multiple variations in the radio light-curve of the colliding wind binary WR 146 (WC6+O): evidence for a third component ⋆

D.Y.A. Setia Gunawan[1,2], **A.G. de Bruyn**[3,1], **K.A. van der Hucht**[2], **and P.M. Williams**[4]

[1] Kapteyn Astronomical Institute, P.O. Box No. 800, 9700 AV Groningen, The Netherlands
[2] Space Research Organization Netherlands, Sorbonnelaan 2, 3584 CA Utrecht, The Netherlands
[3] Netherlands Foundation for Research in Astrophysics, P.O. Box No. 2, 7990 AA Dwingeloo, The Netherlands
[4] Institute for Astronomy, University of Edinburgh, Royal Observatory, Blackford Hill, Edinburgh EH9 3HJ, U.K.

Received 2 September 1999 / Accepted 12 January 2000

Abstract. The Wolf-Rayet star WR 146 (HM19-3, WC6+O) is the brightest WR star at radio wavelengths. We have been monitoring this system with the Westerbork Synthesis Radio Telescope (WSRT) at 1.4 and 5 GHz (21 and 6 cm) since 1989. The time-averaged spectral index $\alpha_{5-1.4\,\mathrm{GHz}} \simeq$ –0.62 clearly points to a domination by non-thermal radiation, which we associate with colliding winds in this binary system. The non-thermal radio flux distribution shows a turn-over at low frequency, which we suggest to be due to free-free absorption of the synchrotron emission from the colliding wind region by plasma around the system.

In the period 1989 – 1997 the average 1.4-GHz flux density increased from $\sim$ 61 to $\sim$ 73 mJy; in the the period 1989 – 1999 the average 5-GHz flux density increased from $\sim$ 29 to $\sim$ 37 mJy. The light-curves show three different kinds of variations: *(i)* a slow linear rise in a time-span of a decade; *(ii)* a 3.38 yr periodic variation; and, *(iii)* rapid non-periodic variations on a time-scale of weeks.

We examine whether the slow rise of the flux density could be explained by decreasing free-free absorption in the line-of-sight through the radiophotosphere of the O component, while moving in an eccentric orbit around the WR component. However, the similarity of the amplitudes ($\sim$ 22% in 10 yr) of the rises at 1.4 and 5 GHz argues against a change in free-free absorption, expected to be strongly wavelength dependent. This points to an intrinsic flux-density variation, possibly due to modulation of the magnetic field strength resulting from orbital motion in a very-long-period eccentric binary system. The relation between the flux-density increase and orbital motion is supported by positional measurements of the 5-GHz data.

We detect a possible motion of the shock zone relative to one of the control sources (Control A) of $\sim 0\overset{''}{.}05$ in the 10 yr observing span. At a distance of 1250 pc this motion corresponds to a projected tangential velocity of about 30 km s^{-1}, which is a plausible orbital velocity for a system like WR 146.

Superimposed on the 1.4-GHz slow rise, we find a sinusoidal variation with a period P = 3.38 $\pm$ 0.02 yr and a semi-amplitude of 4.3 $\pm$ 0.2 mJy. Adopting a distance of 1250 pc to the system and a 162 mas WR+O separation, we consider the observed 3.38 yr period too short to be the WR+O binary period by at least two orders of magnitude. We suggest that the periodic variability is caused by a third, low-mass object, modulating the mass flow and/or the magnetic-field of the O component. Unfortunately, our 5-GHz data are far too few and not adequately spread over the whole phase to confirm that they consistently follow the 3.38 yr period found in the 1.4-GHz data.

The erratic 'micro'-variation in the 1.4-GHz light-curve is about 4σ of the typical 0.5 mJy observational uncertainty, on a time-scale of weeks to months. When irregularities in the mass flow (clumps, inhomogeneities and/or turbulence in the O and/or WR star winds) reach the wind collision region, variation in the non-thermal emission can be expected. Such irregularities can also affect the free-free line-of-sight absorption at the lowest observing frequencies.

Key words: stars: binaries: general – stars: Wolf-Rayet – stars: individual: WR 146 – radio continuum: stars

1. Introduction

The Wolf-Rayet object WR 146 (HM19-3) is projected towards the heavily obscured Cygnus OB2 region. One or more dark clouds in the line-of-sight cause a reddening of E_{B-V} = 2.8 mag towards WR 146 (Willis et al. 1997), in spite of its proximity of d = 1.2 kpc (Dougherty et al. 1996) or even d = 0.75 kpc (Willis et al. 1997). Among the radio WR stars WR 146 is the brightest, although not the most luminous.

Felli & Massi (1991) observed WR 146 with the EVN (European VLBI Network) and the VLA and report a spectral index α = –1 (where the flux density $S_\nu \propto \nu^\alpha$). This clearly points to a non-thermal source, since α = +0.6 is expected theoretically for free-free radiation originating in a stellar wind (Wright & Barlow 1975), and in practice $\alpha \simeq$ +0.7–0.8, depending on the conditions in the wind (see, e.g., Williams 1996). Felli & Massi (1991) suggested that the total radio emission is composed of

Send offprint requests to: (D.Y.A.Setia-Gunawan@astro.rug.nl)

⋆ Based on observations made with the Westerbork Synthesis Radio Telescope (WSRT). The WSRT is operated by the Netherlands Foundation for Research in Astronomy (NFRA) which is financially supported by the Netherlands Organization for Scientific Research (NWO).

thermal radiation from a stellar wind and of a small diameter ($\leq$ 30 mas) non-thermal component. Van der Hucht et al. (1995) and Setia Gunawan et al. (1996), with earlier reductions of the WSRT data available at the time, showed the flux density of WR 146 to be varying at both 5 GHz and 1.4 GHz, with a time-averaged spectral index $\alpha_{5-1.4\,\mathrm{GHz}} \simeq -0.7$. A MERLIN 5-GHz image of WR 146 by Dougherty et al. (1996) resolved WR 146 in two components: a bright northern component ($S_{5\,\mathrm{GHz}}$(N) = 28.5 ± 0.2 mJy) and a weaker southern component ($S_{5\,\mathrm{GHz}}$ (S) = 1.0 ± 0.2 mJy), separated by 116 ± 14 mas. From a Gaussian fit of the visibility, they determined the diameter of WR 146N as 38 ± 1 mas. Their unresolved 1.6-GHz image yields a flux density of $S_{1.6\,\mathrm{GHz}} = 54.49 \pm 0.20$ mJy and thus a spectral index $\alpha_{5-1.6\,\mathrm{GHz}}$ = –0.6.

HST-WFPC2 observations by Niemela et al. (1998) resolved the WR star and its companion in U, B, and V and reported a projected separation of 168 ± 31 mas at the same position angle ($21 \pm 4°$) as the radio images. This binary separation is confirmed by Dougherty & Williams (1999) in a 22-GHz VLA observation. They observed both thermal components of the binary, separated by 162 ± 8 mas, at a position angle of 22°. The WR component of the binary has a flux density of $S_{22\,\mathrm{GHz}}$(S)= 7.0 ± 1.3 mJy, which gives $\alpha_{22-5\,\mathrm{GHz}}$ = +0.74 $\pm$ 0.2, consistent with the $\alpha_{\mathrm{midIR-mm}} \simeq$ +0.78 of Dougherty et al. (1996). The 22-GHz flux-density of the O star is less certain as there may be a contribution from the non-thermal component present in the $S_{22\,\mathrm{GHz}}$(N) of $\sim$ 10 mJy.

Smith et al. (1990) classify the WR star as WC6, as confirmed by Willis et al. (1997). Eenens & Williams (1994) pointed out that WR 146 has broader than usual, flat-topped near-IR emission-line profiles, and that the blue-shifted absorption component of He I 2.058μ yields a 40% higher v_∞ than typical for WC6 stars. Willis et al. (1997) support the finding of broad spectral lines with their slightly wider than normal C IV λ5804Å emission line.

Dougherty et al. (1996) discovered H_γ and H_δ absorption lines in an INT spectrum of WR 146, attributed to an O-type companion of the WC6 star. Willis et al. (1997) classified the O companion as a O8.5V star on the basis of emission line-to-continuum ratios and assumed absolute visual magnitudes, as they did not find absorption lines in their spectrum. Niemela et al. (1998) applied the distances from their HST image and the 5-GHz map of Dougherty et al. (1996) to the colliding wind model of Usov (1992), and derived as spectral type O5-6III-V. From a recent WHT spectrum Dougherty et al. (2000) classify the O star as an O8 type. Observed parameters of WR 146, are listed in Table 1.

It is tempting to compare WR 146 with the archetype colliding wind binary WR 140 (WC7+O4-5), which shows a definite 7.94-yr period in its IR light-curves, optical RV-curve, radio light-curves (Williams et al. 1990, 1994; White & Becker 1995), and in its UV RV-curves (Setia Gunawan et al. 1995a,b). Models proposed therein discuss the variations in terms of modulation, due to eccentric binary motion, of radiation induced by the colliding stellar winds of the two components. The non-thermal radio emission observed is thought to originate in the region where the winds of the WR star and the O-type companion interact. Given the large separation in WR 146, Dougherty et al. (1996) suggested a period of $\sim$ 300 yr for a 30 $M_\odot$ system. The observed radio variability of WR 146, however, shows short-term variations ($\sim$ weeks) and a long-term variation ($\sim$ decade) (van der Hucht et al. 1995; Setia Gunawan et al. 1996; and the present data). Therefore, we re-investigated the available WSRT data, supplemented with more recent data, and reduced them in a homogeneous manner as described in Sect. 2. The light-curves are discussed in Sect. 3. In Sect. 4 we list the parameters and draw the geometry of the system, which are derived and used in the subsequent sections. The origin of the non-thermal radiation is discussed in Sect. 5. The possible causes of the variability seen in the light-curves are discussed in Sect. 6.

Table 1. Observed parameters of WR 146.

parameter		unit	ref.
V	12.80	mag	W1997
$B-V$	2.46	mag	W1997
spectral type WR	WC6		SSM1990
spectral type O	O8		DWP2000
v_∞ (WR)	2 700	km s^{-1}	W1997
$S_{1.1\,\mathrm{mm}}$ N+S	30 ± 8	mJy	D1996
$S_{22\,\mathrm{GHz}}$(WR) S	7.0 ± 1.3	mJy	D1999
$S_{5\,\mathrm{GHz}}$(WR) S	1.0 ± 0.2	mJy	D1996
$S_{5\,\mathrm{GHz}}$(non-thermal source) N	28.5 ± 0.2	mJy	D1996
$S_{1.6\,\mathrm{GHz}}$ N+S	54.5 ± 0.2	mJy	D1996
$\alpha_{\mathrm{midIR-mm}}$	+0.78		D1996
$\alpha_{22-5\,\mathrm{GHz}}$(WR) S	+0.74 $\pm$ 0.2		D1999
$\alpha_{5-1.6\,\mathrm{GHz}}$	–0.6		D1996
$\alpha_{5-1.4\,\mathrm{GHz}}$	–0.62		this work
size thermal source S at 5 GHz	≤ 53	mas	D1996
size non-thermal source N at 5 GHz	38 ± 1	mas	D1996
r_r (5 GHz)	116 ± 14	mas	D1996
r_s (HST optical)	168 ± 31	mas	N1998
r_s (22 GHz)	162 ± 8	mas	D1999
L_X (EINSTEIN-IPC 0.2–4.0 keV)	0.09 ± 0.06	$L_\odot$	P87

Notes: r_r: separation of the thermal and non-thermal sources; r_s: binary separation.
References: D1996: Dougherty et al. 1996; D1999: Dougherty & Williams 1999; DWP2000: Dougherty et al. 2000; N1998: Niemela et al. 1998; P1987: Pollock 1987 (corrected for distance); SSM1990: Smith et al. 1990; W1997: Willis et al. 1997.

2. Observations and data reduction

We have been monitoring the system with the WSRT at 5 and 1.4 GHz since 1989. The WSRT consists of an East-West (E-W) array of fourteen 25 m antennas with a maximum baseline of 2.8 km. Ten of the antennas (telescopes 0 to 9) are fixed at a distance of 144 m from each other, while the other four (telescopes A, B, C and D, with telescope A nearest to telescope 9) are movable on tracks. WR 146 was observed in snapshots of a few hours in filler-time slots and occasionally in full 12^h observing runs. The radio components of WR 146 resolved by MERLIN, cannot

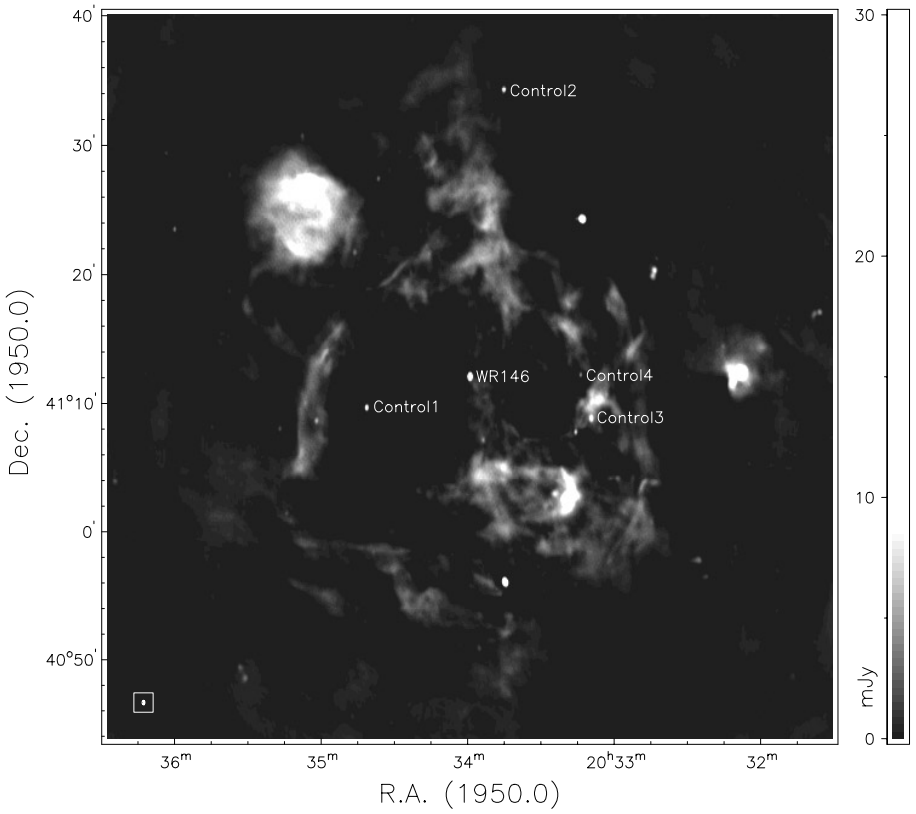

Fig. 1. WSRT 1.4-GHz field around WR 146. The control sources are bright point-sources in the field, used to monitor whether any systematic error in the data is present.

be resolved by the WSRT and thus we observed the total flux density of the binary system.

The WSRT Digital Continuum Backend (DCB, O'Sullivan 1984) has 8 channels or bands which can be set to either 5 or 10-MHz bandwidth. Different DCB settings were used during the 1.4-GHz observations. Until 1990 the 1.4-GHz DCB used 8 adjacent bands of 5 MHz providing a total bandwidth of 40 MHz centred at 1401 MHz, and from 1991 up to 1998 the DCB used pairs of 5 and 10-MHz bands with a total bandwidth of 60 MHz centred at 1395 MHz. A small fraction of the 1.4-GHz data was observed using the Digital Line Backend (DLB, Bos et al. 1981). We use data from the continuum channel of DLB, which has only a 10-MHz bandwidth and is centred at 1412 MHz, and therefore has higher noise. The 1.4-GHz data obtained with these different settings can be safely combined, as the frequency-coverage of the narrower bands was covered by the wider bands and thus the different bandwidths will only affect the noise of the data. As bandwidth smearing at 1.4 GHz is important, data from each band were reduced separately.

The 5-GHz observations used the DCB with a total bandwidth of 80 MHz, centred at 4874 MHz. However, the 1995 5-GHz data were taken with VLBI settings where the backend has a total bandwidth of 58 MHz centred at 4985 MHz. Although these two bands do not overlap with one another, we can combine the data as the spectral index corrections are of the order of the thermal noise. The 1999 5-GHz data was taken using the new Multi Frequency Front End (MFFE) which has a higher sensitivity than the older frontend. The log of observations is presented in Table 2.

The reduction of the data, which includes calibration and mapping, was carried out with the WSRT-NEWSTAR software package (Noordam 1994), and was done in three steps. *First*, after bad data (due to, e.g., interference) were flagged, the data were flux-calibrated. The antenna corrections were obtained from one of the major calibrators: 3C48, 3C147, 3C286 or 3C295 observed right before and/or after the WR 146 observations. Their flux densities are on the scale of Baars et al. (1977), with 3C286 radio fluxes $S_{1400\,\mathrm{MHz}} = 14.77$ Jy and $S_{4874\,\mathrm{MHz}} = 7.42$ Jy. Their relative flux densities are known to within 1% and to be stable at that level. We also made polarization images for the 12^h runs. We find no polarization at 1% level.

Second, we made maps of the field in both wavelength ranges and obtain models that represent the field. We only used data from 40 baselines (i.e., from fixed-movable telescope combinations) of bands with 10-MHz bandwidths to ensure a uniform *uv*-coverage. Some of the 1.4-GHz data were combined to form an as complete as possible *uv*-coverage to make a 4×12^h map: one map obtained with telescopes 9 and A separated at 36 m, the next with 9–A at 54 m, 72 m and 90 m apart. In this way we obtained a map with less disturbance from grating ellipses. This $3.^\circ 2 \times 3.^\circ 2$ map, with a $13'' \times 21''$ beam, was CLEAN-ed using the Högbom-CLEAN algorithm. We then obtained a model which represents the (discrete) point and extended sources in the complicated field around WR 146. Fig. 1 shows the self-calibrated and CLEAN-ed map of the field around WR 146 at 1.4 GHz. The 1.4-GHz field around WR 146 was represented by a model containing 18 point sources and about 15 500 CLEAN

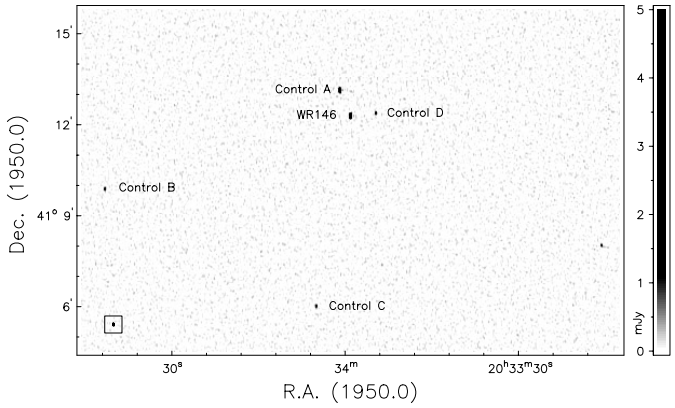

Fig. 2. WSRT 5-GHz field around WR 146. Inverse grey scale is used for clarity.

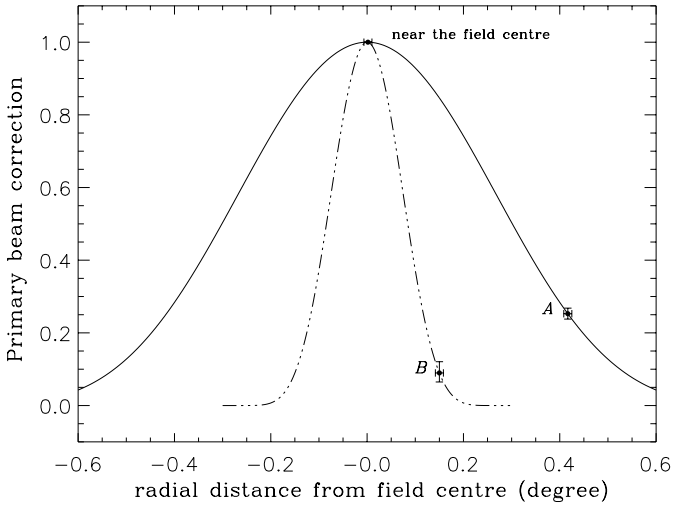

Fig. 3. Primary beam correction for the a typical WSRT antenna at 1.4 (——) and 5 GHz (–...–...). *A* is an object 25′ away from the 1.4-GHz pointing centre, and *B* is an object 9′ away from the 5-GHz pointing centre. A small pointing error will not affect the flux density of objects near the centre of the field but will give a large error on the correction factor for an object near the edge of the primary beam.

components of extended sources, with a total flux of about 7.5 Jy. From the 12^h synthesis 5-GHz data we made a $0.^\circ6 \times 0.^\circ6$ map with a $3.''4 \times 5.''8$ beam (Fig. 2), where we can see none of the complicated extended features present in the 1.4 GHz map. This 5-GHz map was self-calibrated, but did not require any CLEAN. The 5-GHz model of the field consists of only six point sources.

Third, the model visibilities were then compared with the individual observations using the NEWSTAR-UPDATE procedure. The UPDATE procedure tries to fit the flux and position of the small number of discrete sources in the model to the observed visibilities using a least-square fit, the model of the extended sources being unchanged. This requires that the model represents the field very well. During the UPDATE procedure, we have excluded the data from the shortest baselines, i.e., from interferometers 9A, 9B, 8A and 8B, in order to avoid the confusion by the extended sources. This means we only used data from baselines with distances greater than 324m. The UPDATE procedure is iterated until the fit values stabilised. Here the E-W array arrangement presents a slight disadvantage: in short snapshot observations the *uv*-coverage is poor and gives difficulties in the fitting of the field model.

2.1. Noise and pointing errors in the flux measurements

Filler-time observations imply different integration times. For a 12^h observation at 1.4 GHz using 40 baselines and two polarizations, the theoretical thermal noise (5 channels each with a 10-MHz bandwidth) is about 0.06 mJy. This implies 0.15 mJy for a 2^h-observation. However, as we are looking in the galactic plane, the thermal noise, but more importantly the sidelobe confusion noise, are higher than the given value; we consider 0.25 mJy as the typical noise of a 2^h-observation at 1.4 GHz. The 5-GHz theoretical thermal noise of the 80-MHz bandwidth total of the 8 channels, using 40 baselines, two polarizations with 12^h observing time is about 0.07 mJy, which will give about 0.25 mJy for a 1^h-observation. The UPDATE procedure also provides an estimate of the flux and position errors. The error introduced by using different calibrators, is expected to be about 1% of the flux density. However, to be conservative, we adopt a 2% variation. An occasional error of a few percent may occur as a result of extinction during periods of (heavy) rain. This is expected to have occurred no more than 5% of the time.

The primary beam attenuation of each telescope at the WSRT can be, empirically, represented by:

$$S = cos^6(\,c\,\nu\,r\,) \tag{1}$$

where $c = 0.064$, ν is the frequency in MHz, and r is the radial distance from the field centre in degree. Although a Bessel function is actually expected, Eq. 1 fits the primary beam measurements very well up to the first minimum (Bregman 1993). A simply convenient presentation of Eq. 1, accurate down to 20% level, is:

$$S = e^{-\frac{r^2}{2\sigma^2}}, \tag{2}$$

where σ is $15.'5$ at 1.4 GHz and $4.'5$ at 5 GHz. The effect of pointing error to the measured flux density can be quickly derived from the derivative of Eq. 2:

$$\frac{dS}{S} = \frac{r}{\sigma}\frac{dr}{\sigma}. \tag{3}$$

A systematic pointing error is unlikely to exceed 30″; with a typical value of 15″. From Eq. 3, this typical pointing error will yield a ∼3% flux density uncertainty at 1.4 GHz for an object which is 30′ away from the pointing centre. However, the beam size at 5 GHz is much smaller, so that the pointing errors may dominate in the 5-GHz flux density uncertainty. In Fig. 3, we show that a small pointing error of, say $0.'5$, will not affect objects close to the field centre. For objects located near the edge of the primary beam this pointing error can translate into a large error on the primary beam correction value.

We have assumed that the pointing variations of the antennas are random. Therefore, the flux density uncertainty caused by

Table 2. Log of observations.

year	I.T. hh:mm	calibrator	remarks	year	I.T. hh:mm	calibrator	remarks
			1.4 GHz				
1989.958	01:59	3C147	DLB	1994.690	07:10	3C48	
1989.980	11:08	3C147	2 obs.	1994.717	05:09	3C48	
1989.991	02:47	3C48	DLB	1994.731	02:50	3C48	
1990.002	02:03	3C48	DLB 2 obs.	1994.961	07:36	3C147	
1990.014	04:58	3C48	2 obs.	1994.977	05:49	3C147	
1990.057	02:59	3C147		1994.997	04:15	3C48	
1990.501	01:58	3C147		1995.449	02:00	3C286	
1990.531	03:04	3C48		1995.454	03:57	3C48	
1990.583	05:29	3C147		1995.463	00:59	3C48	
1990.616	03:37	3C48		1995.468	00:59	3C48	
1990.657	03:31	3C286	DLB	1995.474	00:59	3C48	
1990.687	05:09	3C286		1995.485	00:54	3C48	
1992.304	01:40	3C147		1995.496	00:52	3C48	
1992.361	01:59	3C286		1995.501	00:57	3C48	
1992.411	01:58	3C286	DLB	1995.512	01:10	3C48	
1992.531	01:59	3C147		1995.520	00:57	3C48	
1992.564	03:59	3C147		1995.531	00:59	3C48	
1992.613	01:58	3C147		1995.591	08:04	3C48	2 obs.
1992.674	01:59	3C147		1995.600	04:29	3C286	
1992.704	01:36	3C48		1995.605	04:29	3C48	
1993.539	01:59	3C147		1995.606	01:08	3C48	
1993.559	02:44	3C147		1995.611	07:30	3C48	
1993.578	01:59	3C295		1995.630	06:56	3C147	
1993.602	01:38	3C286		1995.652	05:51	3C147	
1993.616	01:55	3C147/3C286		1995.668	01:34	3C147	
1993.641	01:59	3C147		1995.690	03:26	3C147	
1993.663	01:59	3C286		1995.706	02:00	3C48	
1993.709	02:00	3C147		1996.381	04:05	3C147	
1993.758	01:30	3C147		1996.419	03:58	3C147	
1993.903	03:55	3C147		1996.490	05:49	3C147	
1993.917	04:34	3C147	DLB	1996.556	05:21	3C48	
1993.936	02:58	3C147	DLB	1997.364	03:55	3C48	
1993.975	02:28	3C48		1997.386	03:09	3C48	
1994.011	01:24	3C48		1997.422	11:05	3C286	
1994.019	02:00	3C147		1997.441	10:19	3C48	
1994.118	02:59	3C48		1997.460	12:00	3C147	
1994.194	02:33	3C48		1997.482	04:39	3C286	
1994.203	04:53	3C295		1997.512	08:38	3C48	
1994.580	04:55	3C48		1997.520	10:25	3C286	
1994.641	04:53	3C48		1997.586	07:54	3C286	
1994.654	06:27	3C48		1997.632	05:55	3C286	
1994.663	03:59	3C48		1997.687	04:58	3C147	
1994.674	05:32	3C147					
			5 GHz				
1989.646	01:13	3C286		1993.129	01:59	3C286	
1989.712	00:59	3C147		1993.471	02:59	3C48	
1989.764	02:00	3C147		1993.493	11:59	3C286	
1989.775	03:19	3C48		1995.405	04:51	3C48	V
1990.348	03:04	3C286		1995.427	03:30	3C286	V
1990.370	00:59	3C48		1995.430	07:35	3C147	V
1990.457	02:59	3C286		1999.260	00:28	3C286/3C48	3 obs.; MFFE
1993.101	01:59	3C286					

note: DLB, MFFE: see text; V = VLBI settings

Table 3. Position and flux densities of WR 146 and the control sources. The flux densities have been corrected for the primary beam. The 5-GHz flux densities of the objects in the 1.4-GHz field were derived from pointed observations to the objects while the other flux densities were derived from the 1.4 and 5-GHz map. The data for the maps and the pointed observations are of different dates and, therefore, the spectral indices may still include effects of variations. Note that Control 1 and Control B are the same object (see text) and that all position errors still have a nominal $0\overset{''}{.}5$ absolute uncertainty.

1.4-GHz field									
object	$\mathrm{RA}_{1.4\,\mathrm{GHz}}(1950.0)$			$\mathrm{DEC}_{1.4\,\mathrm{GHz}}(1950.0)$			$S_{1.4\,\mathrm{GHz}}$	$S_{5\,\mathrm{GHz}}$	$\alpha_{5-1.4\,\mathrm{GHz}}$
	h	m	s	°	′	″	mJy	mJy	
WR 146	20	33	59.07 ± 0.000	41	12	18.38 ± 0.01	70.92 ± 0.71	32.41 ± 0.34	–0.63
Control 1	20	34	41.56 ± 0.001	41	09	53.01 ± 0.03	18.94 ± 0.20	10.90 ± 0.18	–0.44
Control 2	20	33	45.04 ± 0.001	41	34	30.73 ± 0.03	44.16 ± 0.47	10.79 ± 0.18	–1.12
Control 3	20	33	09.21 ± 0.002	41	09	02.17 ± 0.03	15.92 ± 0.17	3.67 ± 0.15	–1.17
Control 4	20	33	13.56 ± 0.003	41	12	24.40 ± 0.09	5.80 ± 0.08	7.60 ± 0.16	+0.22

5-GHz field							
object	$\mathrm{RA}_{5\,\mathrm{GHz}}(1950.0)$			$\mathrm{DEC}_{5\,\mathrm{GHz}}(1950.0)$			$S_{5\,\mathrm{GHz}}$
	h	m	s	°	′	″	mJy
WR 146	20	33	59.09 ± 0.000	41	12	18.60 ± 0.01	32.41 ± 0.12
Control A	20	34	00.91 ± 0.001	41	13	09.00 ± 0.01	21.60 ± 0.12
Control B	20	34	41.57 ± 0.004	41	09	52.92 ± 0.13	18.33 ± 0.91
Control C	20	34	05.02 ± 0.004	41	06	02.33 ± 0.12	6.90 ± 0.36
Control D	20	33	54.69 ± 0.005	41	12	24.12 ± 0.13	2.11 ± 0.23

the combined pointing errors from all telecopes can be brought down from the single telescope value by about a factor of $\sqrt{N_{\mathrm{tel}}}$, where N_{tel} is the number of telescopes involved in each observation.

3. Results

We tried to use the other point sources in the field as control sources, in order to see whether there is any correlation between the variation in the flux density of the control sources and WR 146 and thus to judge whether the variation is intrinsic or due to experimental error.

In Table 3 we have listed the positions and primary beam corrected flux densities of WR 146 and the control sources. $S_{1.4\,\mathrm{GHz}}$ of Control 1–4 and $S_{5\,\mathrm{GHz}}$ of Control A–D were obtained from the primary beam corrected 1.4 and 5-GHz maps, respectively, while $S_{5\,\mathrm{GHz}}$ of Control 1–4 were derived from pointed observations to these objects. We searched the SIMBAD data base and the Digital Sky Survey to identify the control sources, but so far have not found any identification for these objects. From the Faint Images of the Radio Sky at Twenty-cm (FIRST) survey, Helfand et al. (1999) found that 99.9 % of all the catalogued sources were extragalactic. With a total of 437,429 sources observed in an area of nearly 5000 deg^2 with a flux density limit of 0.7 mJy, this gives a number density of 87 extragalactic sources per deg^2. Therefore, it is quite likely that the (un-identified) control sources in our observation are extragalactic as well.

Only one control source is bright enough to be detected in both the 1.4 and 5-GHz maps: Control 1 and Control B are the same object. However, Table 3 shows a different $S_{5\,\mathrm{GHz}}$ for Control 1 and Control B by almost a factor of 2. This is most probably caused by over-estimating the primary beam correction, e.g., due to a small pointing error, as Control B is nearly at the edge of the 5-GHz primary beam.

Linear models were fitted by applying a least-square method to both the 5-GHz and 1.4-GHz data, using their observational errors as weight. These fitted lines were used to obtain the 'average' values in the two datasets. The deviation of the points from the fitted lines were then used to try to find correlations among the objects, where we saw slight correlations between several data points of the 1.4-GHz data, but none in the 5-GHz data. Therefore, we normalized the 1.4-GHz data with the mean of the deviations of the control sources. We did not use Control 4 in the normalization of the 1.4-GHz data, as it is too weak. The flux densities are presented in Fig. 4 and Fig. 5, showing the light-curves of WR 146 and the other point sources in the field.

Linear models were once more fitted, also by least-square method. These are also shown in Fig. 4 and Fig. 5. The standard deviations, σ, of the control sources were already reaching their thermal noise. The flux densities in the light-curve figures are apparent fluxes, i.e., not corrected for the primary beam. This suites our purpose better, where we are only interested in the flux density variations that may occur in the light-curves.

We obtain a time-averaged 5–1.4-GHz spectral index of WR 146, $\alpha_{5-1.4\,\mathrm{GHz}} \simeq$ –0.62, confirming Dougherty et al. (1996), and attribute this to the non-thermal emission in the colliding-winds which will dominate the observed flux in this wavelength range. It is interesting to note that the flux density of Control 1 at 1.4 GHz went slowly down with time, consistent with Control B at 5 GHz. At both 1.4 and 5 GHz, the *rms*

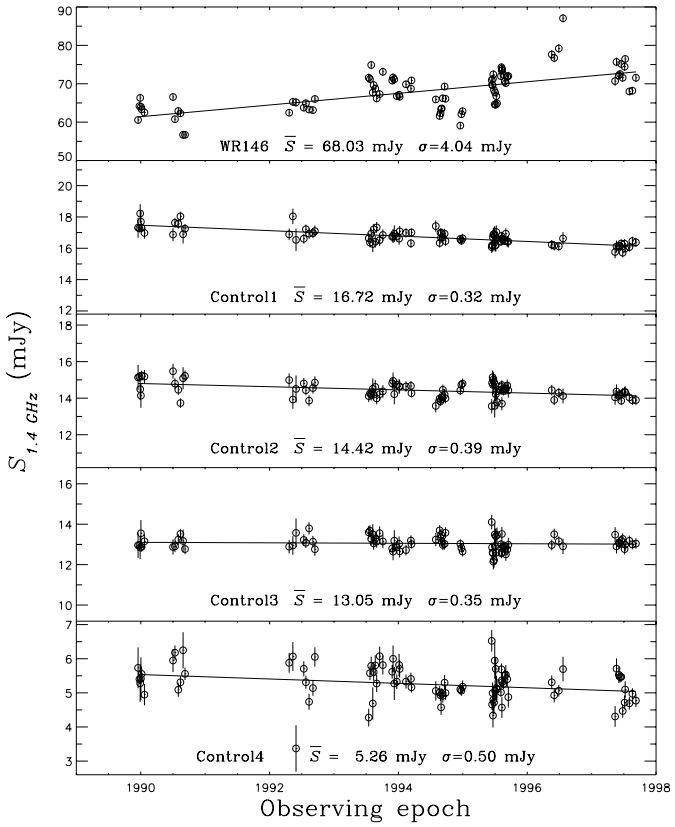

Fig. 4. WSRT 1.4-GHz light-curves. The flux densities were not corrected for the primary beam. The apparent flux density of WR 146, which is in the field centre, is similar to the corrected one. As for the objects away from the field centre, the apparent flux densities are fainter than after correction (see text).

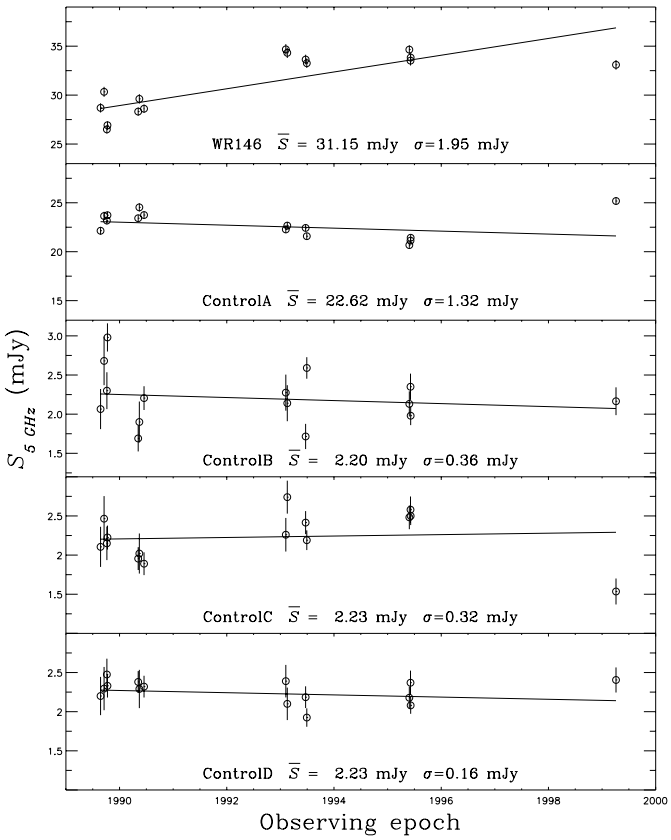

Fig. 5. WSRT 5-GHz light-curves (as in Fig. 4, the flux densities were not primary-beam corrected).

deviations of Control 1 do not indicate any variation. The 5–1.4-GHz spectral index of Control 1, $\alpha = -0.44$, may indicate a non-thermal source. However, an extragalactic origin may not be excluded as we can expect a lot of the source in our field, as mentioned above.

The strong extended emission in the 1.4-GHz field, shown in Fig. 1, is also of great interest, as it may represent matter blown by winds of (massive) stars in the field. The ring-like structure around WR 146 may be related to the faint point source 6′ south of WR 146. The extended emission is and will be discussed in separate studies (Setia Gunawan et al. 1999, and in preparation), where we combine our WSRT 1.4-GHz mosaic observation of the Cygnus OB2 region with an image from the WSRT 350-MHz survey of Vasisht & de Bruyn (unpublished).

4. Geometry of the system

The case of single star *versus* binary star origin of the non-thermal radiation observed from a sizeable fraction of the O-type stars and WR stars, was reviewed by van der Hucht (1992) and van der Hucht et al. (1992), in favour of the colliding winds model. The non-thermal radiation observed in colliding wind binaries is thought to be synchrotron radiation arising from electrons accelerated to relativistic velocities (e.g., Usov 1992). The acceleration mechanism can be by first-order Fermi-acceleration of electrons in shocks, arising in the region where the winds of two components of a massive binary collide (e.g., Eichler & Usov 1993). A second mechanism, acceleration of electrons to relativistic velocities by magnetic field compression in the colliding winds, has been proposed by Jardine et al. (1996).

In the discussion that follows, we will apply the colliding wind geometry of Usov (1992), where smooth spherical winds from the binary components collide at the stagnation point determined by the ram-pressure of the winds. The distances to the stagnation point from each star, $r_{\rm WR}$ and $r_{\rm O}$, depend on the ratio of the wind momenta

$$r_{\rm WR} = \frac{1}{1+\eta^{\frac{1}{2}}}\, D_{\rm WR-O}\,, \qquad r_{\rm O} = \frac{\eta^{\frac{1}{2}}}{1+\eta^{\frac{1}{2}}}\, D_{\rm WR-O} \tag{4}$$

$$\text{with} \quad \eta = \frac{\dot{M} v_\infty({\rm O})}{\dot{M} v_\infty({\rm WR})}\,. \tag{5}$$

The minimum condition that radio emission at a certain frequency can be observed, is that it is radiated from a distance larger than the radiophotosphere at that frequency. For a

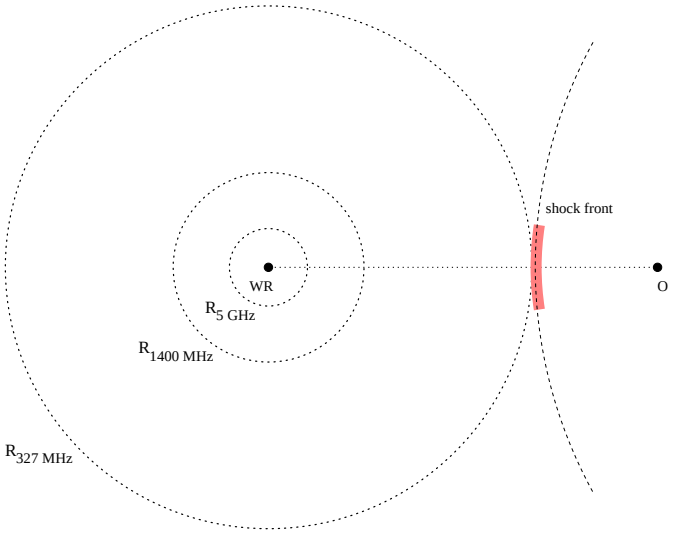

Fig. 6. The face-on view of the geometry of the binary system, assuming a distance of 1250 pc to the system.

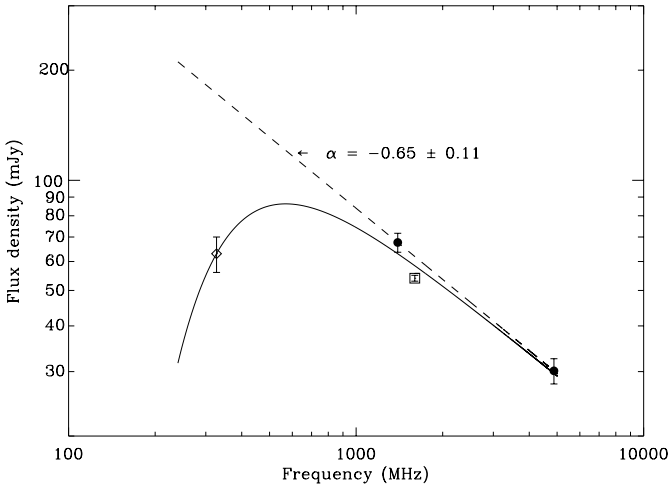

Fig. 7. Non-thermal radio-flux distribution. Dashed line (- - -): the expected synchrotron radiation flux-density curve (without any absorption) with α = –0.65 ± 11; solid line (—): synchrotron radiation with free-free absorption; • = time-averaged 5-GHz and 1.4-GHz WSRT data (this paper), with uncertainties from the *rms* deviation as given in Fig. 4 and Fig. 5; □ = MERLIN 1.6-GHz (Dougherty et al. 1996), with uncertainty ± 1 mJy (Dougherty, private comm.); ◇ = 327-MHz WSRT data (Taylor et al. 1996). The thermal contribution has been subtracted (see text).

smooth, spherical wind of electron temperature $T_{\rm w}$, the radio-photosphere radius is given by

$$R_\nu = 2.8 \times 10^{28}\, Z^{\frac{2}{3}}\, g_{\rm ff}(\nu, T_{\rm w})^{\frac{1}{3}}\, T_{\rm w}^{-\frac{1}{2}}\, \gamma^{\frac{1}{3}} \left(\frac{\dot{M}}{\mu\, v_\infty\, \nu}\right)^{\frac{2}{3}} \ {\rm cm} \quad (6)$$

where Z is the *rms* ionic charge, γ is mean number of electrons per ion, μ is mean molecular weight (Wright & Barlow 1975). The gaunt factor $g_{\rm ff}(\nu, T_{\rm w})$ can be approximated (Leitherer & Robert 1991) by:

$$g_{\rm ff}(\nu, T_{\rm w}) = 9.77 \left[1 + 0.13 \log\left(\frac{T_{\rm w}^{\frac{3}{2}}}{Z\nu}\right)\right]. \quad (7)$$

Taylor et al. (1996) observed the emission from WR 146 at 327 MHz. For the WC6 star, using Z = 1.2, γ = 1.15, μ = 5.29, $T_{\rm w}$ = 8 000 K as in Willis et al. (1997), we obtain $R_{327\,\rm MHz}$ = 142 AU. This has to be the minimum distance associated with the 116 mas separation between the WR star to the non-thermal source, in order to be able to observe the 327-MHz emission, as a shorter distance will put shock front within $R_{327\,\rm MHz}$ of the WR component. Therefore, we suggest that the minimum distance to the binary system WR 146 is 1250 pc, in accordance with Dougherty et al. (1996). The geometry of the system at this distance is shown in Fig. 6.

The colliding wind model gives also constraints on the parameters of the O component of the binary. The HST projected binary separation of 168 mas and the 5-GHz $r_{\rm WR}$ distance of 116 mas give a distance ratio $r_{\rm O}/r_{\rm WR}$ = 0.45, resulting in $\dot{M} v_\infty({\rm O}) = 0.2\, \dot{M} v_\infty({\rm WR})$. Niemela et al. (1998) suggests that only a combination of $\dot{M}_{\rm O}$ and v_∞(O) from an O5-6III-V type star can result into the observed distances. This is an earlier type than late O-type suggested by Dougherty et al. (1996), the O8.5V classification by Willis et al. (1997), and the recent O8 classification by Dougherty et al. (2000). Anyhow, we try to accommodate a broad spectral classification range, and thus a wide range of masses and luminosities for the O compoment. The adopted and derived parameters (as well as those derived in the following sections) are listed in Table 4.

5. Origin of the non-thermal radiation

Dougherty et al. (1996) measured the 5-GHz thermal emission of WR 146S to be 1.0 ± 0.2 mJy. With a free-free spectral index of α = +0.67 the thermal emission at other frequencies are expected to be: $S_{1.6\,\rm GHz} \simeq 0.5$ mJy, $S_{1.4\,\rm GHz} \simeq 0.4$ mJy and $S_{327\,\rm MHz} \simeq 0.2$ mJy. Subtracting these thermal contributions from our time-averaged 5 and 1.4-GHz flux densities, the 1.4-GHz data of Dougherty et al. (1996) and the 327-MHz data of Taylor et al. (1996), we obtain the non-thermal radio flux densities of WR 146 as shown in Fig. 7. It should be noted that the 327-MHz observation of Taylor et al. is a time-average of 1984–1985 and 1988–1990 data.

Assuming that the energy density of the relativistic particles has a power law distribution, $N(E)\, dE = K E^{-\gamma} dE$, where K is a constant, the synchrotron flux density will depend on frequency according to $S_\nu \propto \nu^\alpha$, where $\alpha = -(\gamma - 1)/2$. If we assume that the flux densities at 5 and 1.4 GHz are purely of synchrotron radiation origin, then the time-averaged non-thermal spectral index is $\alpha_{\rm NT} = -0.65 \pm 0.11$, which yields γ = 2.3. This is slightly higher than the value for Fermi-acceleration in a strong adiabatic shock (γ = 2, Bell 1978). Such a difference from the theoretical value is quite often observed. However, the 327-MHz flux is much lower than expected from extrapolation of the power-law spectrum; below we consider possible reasons for this.

Table 4. Adopted and derived parameters used in the analysis, based on assumptions and/or modelling.

	WR	O	unit
spectral type	WC6 [a]	O8 [b]	
M	15 [c]	15 – 60 [d]	$M_\odot$
$\dot{M}$	2.6×10^{-5} [e]		$M_\odot\,yr^{-1}$
v_∞	2700 [e]		$km\,s^{-1}$
γ	1.15 [e]		
μ	5.29 [e]		
Z	1.2 [e]		
T_w	8000 [e]		K
g_{ff}(5 GHz)	4.8		
g_{ff}(1.4 GHz)	5.5		
g_{ff}(327 MHz)	6.3		
$R_{5\,GHz}$	21		AU
$R_{1.4\,GHz}$	51.5		AU
$R_{327\,MHz}$	142		AU
T_*	49 000 [f]	43 000 – 23 500 [d]	K
R_*	5 [f]	7 – 16 [d]	$R_\odot$
$\log(L_*/L_\odot)$	5.1	4.8 – 5.2	
L_*	5×10^{38}	$2.7 - 5.2 \times 10^{38}$	$erg\,s^{-1}$

Notes:
a. Smith et al. 1990; b. Dougherty et al. 2000; c. Smith & Maeder 1989;
d. Conti 1988 (values for 05 - 09.5); e. Willis et al. 1997; f. Koesterke & Hamann 1995.

Estimated distance to the binary system:			
Dougherty et al. (1996)		1200	pc
Willis et al. (1997)		750	pc
Niemela et al. (1998)		1700	pc
Dougherty et al. (2000), from the distance modulus		1380	pc
minimum distance to observe the 327 MHz radiation		1224	pc

distance		750 pc	1250 pc	unit
observed $v_{orb.}$ of 5 mas yr^{-1}		17.8	30	$km\,s^{-1}$
r_{5GHz} (116 mas)		87	145	AU
D_{WR-O} (168 mas)		126	210	AU
size of non-thermal source (38 mas)		29	46	AU
Circular orbit:				
M_{WR+O} = 30 $M_\odot$:	P_{min}	258	556	yr
	v_{orb}	14.5	11.2	$km\,s^{-1}$
M_{WR+O} = 75 $M_\odot$:	P_{max}	163	351	yr
	v_{orb}	23	17.8	$km\,s^{-1}$
Elliptical orbit:				
M_{WR+O} = 30 $M_\odot$:	e_{min}	0.21	0.75	
	v_a	12	4	$km\,s^{-1}$
	v_p	18	30	$km\,s^{-1}$
M_{WR+O} = 75 $M_\odot$:	e_{min}	0.25	0.48	
	v_a	18	11	$km\,s^{-1}$
	v_p	30	30	$km\,s^{-1}$
n_e(WR) at shock front		32 500	11 700	cm^{-3}
B_{Razin} for $\nu_{Razin} = 1.4$ GHz		464	167	μGauss
t_{IC}		4.7×10^7	7.7×10^7	sec
		1.5	2.4	yr
Photon energy density at the shock front:				
• due to WR star:		7.8×10^{-4}	2×10^{-4}	$erg\,cm^{-3}$
• due to O star: for $\log(L_{min}/L_\odot)$ = 4.8		4.2×10^{-4}	1.5×10^{-4}	$erg\,cm^{-3}$
for $\log(L_{max}/L_\odot)$ = 5.2		8.1×10^{-4}	2.9×10^{-4}	$erg\,cm^{-3}$
Magnetic energy density for $B = B_{Razin}$		8.6×10^{-9}	1.2×10^{-9}	$erg\,cm^{-3}$

5.1. Free-free absorption

In a configuration where a region containing relativistic electrons is surrounded by a thermal plasma, like that in the colliding winds region of WR 146 system, the synchrotron radiation will be suppressed by thermal absorption in the plasma. With the absorption coefficient in the radio range following the relationship $\kappa_\nu = l\nu^{-2.1}T^{1.35}$, where l is the extent of plasma along the line-of-sight (Mezger & Henderson 1967), the resulting flux density will be of the form: $S_\nu \propto \nu^\alpha e^{C\nu^{-2.1}}$.

We tried to fit the time-averaged 5000, 1400, and 327-MHz WSRT flux densities and the 1600-MHz MERLIN data by power-law synchrotron emission, which includes free-free absorption, of the form

$$S_\nu = S_{327\,\mathrm{MHz}} \left(\frac{\nu}{327}\right)^\alpha e^{\left(-\tau_0\,\nu^{-2.1}\right)} \tag{8}$$

where S_ν is flux density at frequency ν, $S_{327\,\mathrm{MHz}}$ is the synchrotron-only flux density at 327 MHz, both in mJy, ν is in MHz, and τ_0 is the optical depth at 1 MHz.

With the four limited data points that we have, we obtain a best fit with $\chi^2 = 0.69$, which gives $\alpha = -0.64$, $\tau_{327\mathrm{MHz}} = \tau_0 \times 327^{-2.1} = 1$, and $S_{327\,\mathrm{MHz}} = 166$ mJy. The spectral index of the fit is within the error of that of the time-averaged 6 and 1.4-GHz non-thermal flux densities ($\alpha_{\mathrm{NT}} = -0.65 \pm 0.11$). With the above fit we expect the spectral index to turn over at $\nu \simeq 570$ MHz.

5.2. Razin effect

White & Chen (1995) and the references therein reminded us that the Razin-Tsytovich effect can be significant. If the density of the thermal plasma is sufficiently large, or the magnetic field is not strong enough the low-frequency synchrotron radiation may be suppressed. The cut-off frequency, ν_R, will occur (Pacholczyk 1970) at

$$\nu_R \simeq 20\frac{n_e}{B} \quad \mathrm{Hz} \tag{9}$$

where n_e is the electron density in cm^{-3}, B is magnetic field in Gauss. The electron density in the interaction region can be derived from the mass-loss, $\dot{M}$, and terminal velocity, v_∞, of the (WC6) wind:

$$n_e = \frac{\dot{M}}{4\,\pi\,r^2\,v_\infty\,\mu\,m_H} \quad \mathrm{cm}^{-3} \tag{10}$$

where r is distance of the WR star to the interaction region in cm, and m_H is the mass of a hydrogen atom. In order to be able to observe the 1.4-GHz radiation, the required minimum magnetic field at the interaction region is 0.17 mG. The Razin-effect may become important if the magnetic field is lower than 0.7 mG, as the 327-MHz will be suppressed. The observed low-frequency downturn could therefore result if the local magnetic field had an intermediate value, i.e., in the range of $0.17\mathrm{mG} < B < 0.7\mathrm{mG}$.

5.3. Synchrotron self-absorption

Synchrotron emission may also become self-absorbed. At optically thick frequencies, this absorption will change the flux-density distribution to a $\nu^{2.5}$ power-law. The critical frequency for synchrotron self-absorption is

$$\nu_{\mathrm{sa}} \simeq 2.145 \left(\frac{S_{\nu_{\mathrm{sa}}}}{\theta^2}\right)^{\frac{2}{5}} B^{\frac{1}{5}} \quad \mathrm{MHz} \tag{11}$$

where $S_{\nu_{\mathrm{sa}}}$ is the maximum flux density in mJy, θ is the size of the source in arcsec, and B is the magnetic field strength in Gauss (Williams 1963).

If we assume that the critical (turn-over) frequency in WR 146 due to synchrotron self-absorption is 600 MHz, then, extrapolating from the synchrotron flux density relation, $S_\nu \propto \nu^{-0.65}$, we obtain $S_{\mathrm{sa}} = 118$ mJy. From Eq. 9, the minimum magnetic field required to observe the 600-MHz radiation is 0.39 mG. Applying the values to Eq. 11, the size of the source is $\theta \simeq 1.3$ mas. The equation

$$T_{\mathrm{b}} = 1.037 \times 10^{-2} \left(\frac{S_\nu}{\nu^2\,sin^2\theta}\right) \quad \mathrm{K} \tag{12}$$

with S_ν is in mJy, gives a brightness temperature of $T_{\mathrm{b}} \simeq 8 \times 10^{10}$ K. From the 5-GHz image of Dougherty et al. (1996) we obtain that the diameter of the non-thermal northern source WR 146N is 38 mas and that the flux density is 28.5 mJy. These give a brightness temperature of 1.37×10^6 K, which is a factor of 10^5 lower than the temperature required for synchrotron self-absorption to take place. Therefore, we discard synchrotron self-absorption as the mechanism responsible for the low frequency absorption observed in Fig. 7.

Unless the magnetic field is known, it is hard to separate whether the turn-over is due to Razin-Tsytovich suppression or to a free-free absorption by a screen in the line-of-sight. The magnetic field of the system is also likely to be difficult to measure due to the turbulence of the particles. However, monitoring at the frequency around the turn-over may be able to solve this problem. If the electron density and/or magnetic-field strength in the colliding wind region changed, e.g., due to binary movement, as will be shown in Sect. 6.1, we will observe change of the turn-over frequency due to the change of the Razin cut-off frequency (Eq. 9). We expect that this will not happen with a free-free absorption by a screen in the line-of-sight.

The four data points in Fig. 7 are also insufficient to obtain good fitting statistics to the model above. Moreover, the three WSRT data are time-averaged values and thus may be contaminated by any variability that occurred during the time span of the observations. Clearly, to be able to constrain our model of WR 146 we need simultaneous observations at several frequencies.

6. Variability of the 5-GHz and 1.4-GHz flux densities

The WR 146 flux densities presented in Fig. 4 and Fig. 5 are larger than the flux densities of the thermal source of WR 146 as calculated in Sect. 5 by, a factor of 30 at 5 GHz and 175

at 1.4 GHz. Their *rms* deviations are higher by a factor of 2.4 and 10, respectively. Therefore we are confident that the observed variations are attributable only to the non-thermal source. We identify three different kinds of variability apparent in the WR 146 binary system:

6.1. The long-term variability

From a linear fit of the light-curve of WR 146 (Fig. 4 and Fig. 5) we find that the 1.4-GHz flux density increased from ∼61 mJy to ∼73 mJy in the period 1989–1997. During the period 1989–1999 the 5-GHz flux density increased from ∼29 mJy to ∼37 mJy. This means that both the 5 and 1.4-GHz flux densities show a similar increase of about ∼ 22% in 10 yr. Using the geometry as in Eichler & Usov (1993), we offer two possible explanations, both in connection with a slow change in the configuration of the system:

6.1.1. Extinction by radiophotosphere

The 1.4-GHz flux density rise may be caused by a reduction in the absorption along our line-of-sight to the emission region with a slow change in the geometry due to the WR+O binary motion.

Let us consider the geometry as in Fig. 6. If the projected separation of the binary components to the stagnation point is smaller than the radiophotosphere, then the non-thermal emission from the stagnation point will be free-free absorbed by the plasma in the radiophothosphere.

At 1250 pc, the 1.4 and 5-GHz radiophotospheres of the WR component are much smaller than $r_{\rm WR}$. On the other hand, $r_{\rm O}$ is smaller than $r_{\rm WR}$. As discussed in Sect. 4, $\dot{M}$ and v_∞ of the O component are not so much different from those of the WR component. Taking reasonable values of $T_{\rm w},\ \mu,\ Z,\ \gamma$ for the O component, the radiophotospheres of the O component are not much smaller than those of the WR component. Therefore, the non-thermal emission may be absorbed by the radiophotosphere of the O star.

However, the amount of absorption can only change if $r_{\rm O}$ changes and this is only possible if the orbit of the WR 146 system is eccentric. In this picture, the flux density will go down to a minimum as the shock front goes within the radiophotosphere of the O star, and returns to its 'normal' level as it emerges at the other side of the radiophotosphere.

As can be derived from Eq. 8, the lower the frequency, the bigger the degree of absorption. But this is not what we observe in Fig. 4 and Fig. 5, where at both 1.4 and 5 GHz the flux-densities vary by ∼ 22%. Therefore, we offer the following possibility.

6.1.2. Intrinsic flux density rise

Eichler & Usov (1993) calculated the expected value of the non-thermal radio luminosity from the region of stellar wind collision, where smooth, spherical stellar winds are assumed, to be

$$L_{\rm NT} \simeq \epsilon\beta\zeta \frac{\dot{M}_{\rm WR} v^2_{\infty,\rm WR}}{2} \left(\frac{\theta^2}{16} + 0.22\eta \frac{v_{\infty,\rm WR}}{v_{\infty,\rm O}}\right) \quad (13)$$

where ϵ is the cosmic-ray partial pressure, β is high-energy electrons efficiency, ζ is the synchrotron emission efficiency, and θ is related to the geometry of the shock-cone formed by the colliding winds. In a shock region with very high Mach number ($\sim 10^2$) both β and ϵ are expected to be nearly constant (Usov, priv. comm.). The luminosity is then related to the separation of the binary components through the synchrotron efficiency ζ, with

$$\zeta \ \propto\ \eta B^{\frac{3}{2}} v^{-1}_{\infty,\rm WR} \nu^{\frac{1}{2}} D_{\rm WR-O}, \quad (14)$$

or

$$L_{\rm NT} \ \propto\ B^{\frac{3}{2}} D_{\rm WR-O}. \quad (15)$$

At distances greater than the Alfven radius ($\sim 3R_*$) from a star B varies inversely with distance form the star (Weber & Davies 1967; Eichler & Usov 1993). Therefore, for the WR+O binary, $B \propto D^{-1}_{\rm WR-O}$. With constant mass-loss rates and terminal velocities we get

$$L_{\rm NT} \ \propto\ D^{-\frac{1}{2}}_{\rm WR-O}. \quad (16)$$

Using this relation, the 22% flux density increase in 10 yr as seen in Fig. 4 and Fig. 5 translates to a 33% decrease in separation between the WR and O components. With the 168 mas HST measurement, the separation change in 10 yr is 55 mas, or 5.5 mas/yr. At 1250 pc this corresponds to 30 km s^{-1}. This variation could be caused by possible eccentricity of the orbit of the WR+O system. The minimum eccentricity required for a binary system with a total mass between 30–75 $M_\odot$ and a binary separation of 210 AU, to be able to have a $v_{\rm orb}$ = 30 km s^{-1}, is between 0.5–0.8. While the WR and O stars approach periastron in such an eccentric orbit, the separation between them decreases, resulting in an increase of the magnetic field strength at the shock region, as does the synchrotron emission and hence the non-thermal luminosity.

There is also other independent evidence for this orbital movement. The angular resolution, $\triangle\theta$, is proportional to the beam size and the inverse of the signal-to-noise ratio ($\frac{S}{N}$), with

$$\triangle\theta \ \simeq\ \frac{HPBW}{2\,(S/N)}. \quad (17)$$

Taking advantage of the small 5 GHz beam and the long time span of the observation period, we tried to detect any motion of WR 146. For the 12^h WSRT 5-GHz observation the accuracy is $\sim 0\overset{''}{.}02$. An object at 1250 pc distance moving with a tangential velocity of 30 km s^{-1} will travel $0\overset{''}{.}05$ in 10 yr, a movement which should be detectable by the WSRT.

We combined the 5-GHz data from each year to improve the $\frac{S}{N}$ and measured the differential position between WR 146 and Control A, which lies about 50″ N and 27″ W of WR 146. The result, shown in Fig. 8, suggests a $0\overset{''}{.}06$ movement of the WR+O system away from Control A in a time span of 10 yr, i.e., 6 mas/yr.This value is similar to what we obtain when translating

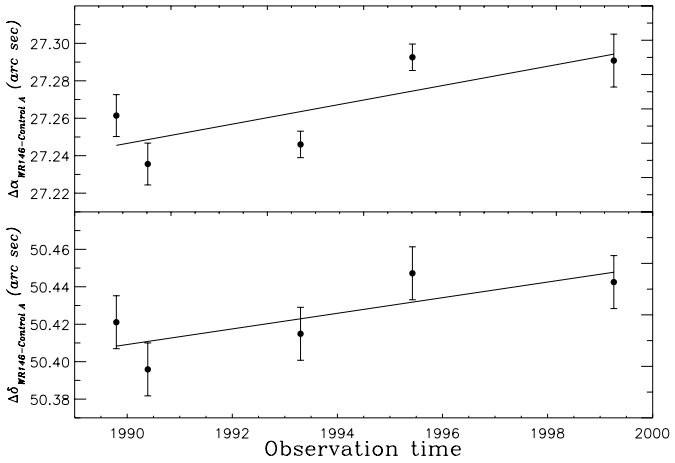

Fig. 8. The change of differential angular distance between WR 146 and Control A, from 5-GHz observations: $\triangle\alpha = 0\overset{''}{.}049$ and $\triangle\delta = 0\overset{''}{.}039$.

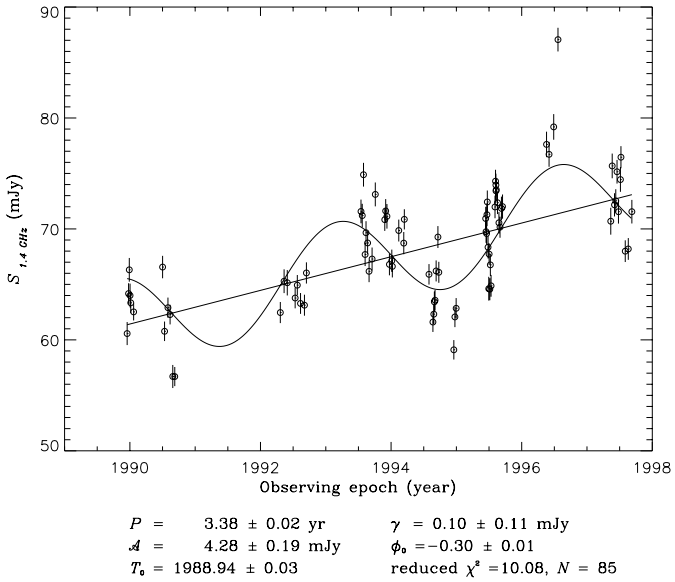

Fig. 9. Periodic variation seen on the 1.4-GHz data of WR 146.

the flux-density increase into a $D_{\rm WR-O}$ decrease, as mentioned above!

However, we have to take into account that the proper motion due to galactic rotation ($\mu_\ell = \frac{A\cos(2\ell)+B}{4.74}$, with $A = 14.82\,{\rm km\,s^{-1}\,kpc^{-1}}$ and $B = -12.37\,{\rm km\,s^{-1}\,kpc^{-1}}$, Feast & Whitelock 1997) at the direction of WR 146 and Control A is about $0\overset{''}{.}005\,{\rm yr}^{-1}$ in the direction of decreasing ℓ, which means $-0\overset{''}{.}05$ during the 10 yr time span.

At this point it is important to know the nature of Control A. If Control A is a galactic source in the same field as WR 146, galactic rotation should not influence the relative distance of WR 146 to Control A. This means that the $0\overset{''}{.}06$ differential movement we observe is the vector sum of their respective motions (away from each other). If Control A is an extragalactic source, the observed movement may all be due to galactic rotation. We obtain the 1.4-GHz flux density of Control A from our 1.4-GHz map, which is 1.2 ± 0.3 mJy. This gives a spectral index, $\alpha_{5-21} = +2.3$. Control A could be a H II region or, given the likelihood of the control sources to be extragalactic as mentioned in Sect. 3, it could be an extragalactic source; both should not vary on a short time-scale. If Control A is an H II region, and if it is at the same distance as WR 146 (which is not unlikely, considering the richness of the field), then the movement of WR 146 relative to Control A may be due to binary motion of the components of WR 146. Further observation of Control A should be able to constrain the origin of Control A better and hence to confirm the binary motion.

With the similar percentages of the flux-density variations at 5 and 1.4 GHz, the large $r_{\rm WR}$ and $r_{\rm O}$, and the yet uncertain wind parameters of the O component, the intrinsic variation discussed above is quite appealing. However, the slow variation that we observed may also be a combination of both varying magnetic-field and change in thefree-free absorption in the line-of-sight.

6.2. Periodic variability

We have tried a periodicity test for the 1.4-GHz data using the STARLINK PERIOD-package version 4.2 (Dhillon & Privett 1997) by employing a Lomb-Scargle Normalized Periodogram, which is a Fast Fourier Transform for unevenly sampled data (Press et al. 1992; Horne & Baliunas 1986). The data were first detrended by the linear fit to avoid very short frequency peaks due to very long term variation. Subsequently, a periodicity test was performed which includes randomisation of the data with 250 permutations. The periodogram of the detrended data shows a high peak corresponding to a period of 3.38 ± 0.02 yr with a very small false alarm probability ($< .01\%$). We fold the data to this period and fit a sinusoid to the folded data. The resulting light-curve and the parameter of the fit can be seen in Fig. 9.

We have also folded the 5-GHz data to the 1.4-GHz period and then tried to fit a sinusoid to the folded data. However, the small number of the data and their inadequate spread over the phase, did not give a good fit. Clearly, more 5-GHz data are needed to see whether WR146 show similar period with that of the 1.4-GHz period.

The periodicity suggests the presence of a regular "clock" modulating the observed flux and one candidate is the influence of binary motion on the intrinsic emission through, e.g., the magnetic field strength.

Near the star, i.e., up to $\sim 3R_\star$, the magnetic field strength B varies with the inverse square of the distance (see Weber & Davies 1967; Eichler & Usov 1993), and Eq. 16 becomes:

$$L_{\rm NT} \propto D_{\rm WR-O}^{-2}. \qquad (18)$$

According to Fig. 9, the 1.4-GHz flux density of WR 146 varies with a 4.3 mJy semi-amplitude, or by about 13% peak-to-peak. This 13% flux-density fluctuation (i.e., luminosity fluctuation) translates to a change of 6% in the separation between the WR and O components (δr). If we adopt the HST WR–O separation of 168 mas, the separation fluctuation is 10 mas, corresponding to 12.5 AU at 1250 pc distance. If a third component is present in

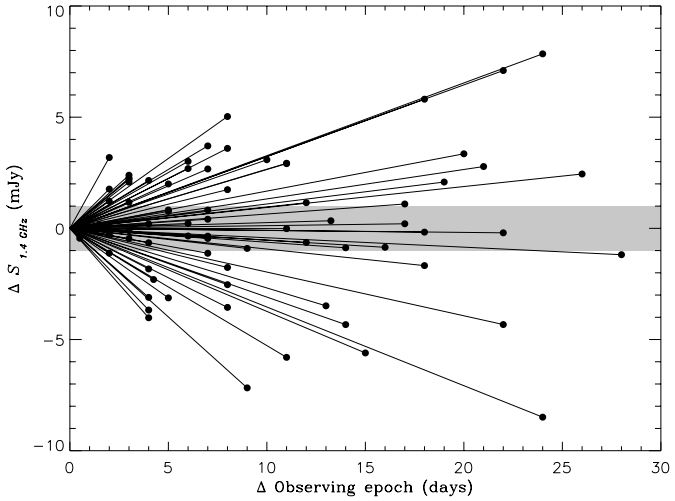

Fig. 10. The 'micro'-variation seen after subtracting the linear long-term trend and the 3.38 yr. sinusoidal variation from the 1.4-GHz light-curve of WR 146. The limit of the shaded area is the highest noise level of the data. More than 2/3 of the data lie outside the shaded area.

the system and orbits either the O star or the WR star, applying the 3.38 yr period and a (12.5/2) AU semi-amplitude to Kepler's third law, we get a total mass of the O+3^{rd} or WR+3^{rd} system to be $\sim 22\,\mathrm{M}_\odot$. If the mass of the 3^{rd}-body is $< 7\,\mathrm{M}_\odot$, the derived total mass is reasonable in combination with $M_{\rm WR}$ or $M_{\rm O}$. However, the shock zone is further away than $\sim 3R_\star$. Therefore, the magnetic field may vary with $D^{-m}_{\rm WR-O}$, where $1 < \mathrm{m} < 2$, which will result in a much bigger mass of the 3^{rd} body. The complication of this model is that if the magnetic field vary with with m close to unity, the mass of the 3^{rd} body can become too big to be real.

A less complicated model is the presence of a low-mass close companion with a significant magnetic field which modulates the flux as it orbits around either the O or WR star. Also, the presence of a close companion to either WR or O stars would affect its mass flow, which could, depending on the geometry, determine the mass flowing into the wind collision region and non-thermal emission. The observed, almost perfect, sinusoid is more likely due to the magnetic field modulation, as this process depends less strongly on the geometry. As $r_{\rm O} < r_{\rm WR}$, $\delta r/r_{\rm O} > \delta r/r_{\rm WR}$, the variation due both to magnetic field or mass flow modulation, will have the biggest effect if the third body is orbiting around the O star rather than around the WR star.

6.3. 'Micro'-variability

There remains a rapid variation in the 1.4-GHz light-curve after we subtract the linear trend seen in the light-curve of WR 146 (Fig. 4) and the 3.38 yr period sinusoid (Fig. 9). In Fig. 10 we have plotted the change of flux densities *versus* time, i.e., between two consecutive observations observed in less than one month. The rapid variation does not follow a Normal distribution, with more than 2/3 of the data lies outside the 1σ –a conservative value of about 2% of the observed flux density as mentioned in Sect. 2.1.

We interpret the lines connecting the origin of the graph (0,0) and the points to be the 'velocity' of whatever process that caused the variation. The steepest of these lines has a gradient of $\sim 1.5\,\mathrm{mJy\,d^{-1}}$. As the total flux density of the thermal source at 1.4 GHz is lower by a factor of 3.7 than the total micro-variation, the change can only be attributable to the non-thermal source. The micro-variation amplitude per day is $\sim$ 2.2% of the 1.4-GHz non-thermal emission at most. Another interesting feature in Fig. 10 is that the changes are almost symmetric, i.e., the rate of flux increase and decrease are the same.

A flux-density increase means simply that there is an increase in synchrotron production. This can be caused by, e.g., density excess in the wind when entering the collision shock-front. However, there are several mechanisms that can be responsible for a flux-density decrease: synchrotron losses, inverse Compton (IC) losses or absorption.

The life-time of relativistic electrons due to synchrotron losses is (Pacholczyk 1970):

$$t_{\rm S} = \frac{1}{2.37 \times 10^{-3}\, E\, H^2} \quad \mathrm{sec} \tag{19}$$

Relativistic electrons moving in a magnetic field strength of 0.167 mG and radiating at a synchrotron characteristic frequency of 1.4 GHz have an energy of about 1.2×10^{-3} erg. For these electrons we obtain a synchrotron life-time of more than 4×10^5 yr. Therefore, the rapid, symmetric flux density decrease cannot be due to the synchrotron relaxation time.

The life-time of particles against IC losses is about 5 orders of magnitude shorter than the lifetime against synchrotron losses (see the energy densities in Table 4) which implies a loss time of about 1 yr. Hence we deduce that even IC losses probably can not explain the rapid decay times observed. However, the energy of the relativistic electrons derived previously, has a Lorenz factor of $\gamma_L \simeq 1400$. The WR star, adopting T_* = 49 000 K, has stellar photons which peak at $\sim$ 12 eV. These photons may be IC scattered to a final energy of $E_{\rm f} = \gamma_L^2 E_i$. This calculation makes clear that there should be a considerable inverse Compton hard X-ray to γ- ray flux ($\sim 10^{33}$ erg s^{-1} or more).

Perhaps the time-scale of the micro-variations represents the time needed for the shocked region to re-adjust to small variations in the mass inflow into the shock zone. Let us simplify the shock-cone model by assuming that the non-thermal emission to originate from a disk of 38 mas diameter (the diameter observed by Dougherty et al. 1996) and 5 mas thickness. The 2% flux density change per day corresponds to a change of a diameter of $\sim$113 mas d^{-1}, which corresponds, at 1250 pc distance, to ~ 141 AU d^{-1}. This corresponds to an equivalent of velocity of $\sim 2.4 \times 10^5$ km s^{-1} (= 0.8 c). This equivalent velocity is much too fast to be the wind velocity of either star in the binary system. We can now turn the argument around: how thin should the region be in order to create the 2% per day increase that is caused by the wind moving at v_∞(WR) = 2700 km s^{-1} (= 1.6 AU d^{-1} or, at 1250 pc, 1.3 mas d^{-1}). This results in a volume of 65 mas^3 which gives a thickness of 0.01 mas to our 38 mas diameter

disk. Therefore, we suggest that the 'micro'-variation may tell us about the size of the irregularities in the mass inflow.

Inhomogeneities or clumpiness in the wind of the WR and/or O star can be responsible for this density changes. When clumps arrive at the shock-front of the colliding-wind system WR146, they deliver extra 'fuel' to the fire and affect the non-thermal radiation generation. However, if the clumps are somewhere in the wind, they can also change the free-free line-of-sight absorption if they are large enough. The effect of clumps in the wind has also been observed, mainly, on the optical spectra of several WR stars (e.g., Lépine & Moffat 1999, Moffat 1996).

7. Summary and future work

In this paper we have discussed the mechanism responsible for the observed suppression of the synchrotron emission from WR 146 at low frequencies. This can be either due to the region of the relativistic particles, i.e., where the winds of the WR and O components collide, being surrounded by thermal plasma causing a free-free absorption or caused by Razin-Tsytovich suppression. Synchrotron self-absorption cannot be responsible for the absorption observed, as the non-thermal source is not compact enough and the temperature of the non-thermal source is too low for the mechanism.

From the 5 and 1.4-GHz WSRT data the Wolf-Rayet system WR 146 showed three kinds of variations:
i) a long term variation, which we assign to the (eccentric) WR+O orbital motion;
ii) a periodic (P = 3.38 yr) variation, which may be due to a third body;
iii) a rapid non-periodic variation, which may be related to inhomogeneities in the stellar winds.

To further test the above conclusions, additional observations are needed:
i) simultaneous observations across the radio spectrum to constrain the non-thermal model applicable to the binary system, e.g., using the MFFE of the WSRT which covers the frequency range between 250 to 8650 MHz and the Giant Meter Radio Telescope (GMRT) at 150 MHz;
ii) a VLBI observation to resolve the system, especially at long wavelength (around 1.4 GHz) to determine the geometry of the system;
iii) monitor the system monthly at 5 and 1.4 GHz, to obtain a better light-curve and thus orbital parameters, and to confirm the motion seen at 5 GHz in Fig. 8;
iv) monitor the system especially at 1.4 GHz in the long term, to constrain the mechanism responsible for the long-term flux-density rise; and
v) obtain optical and infrared radial velocity curves, in order to derive the orbital parameters of the 3.38 yr system.

Acknowledgements. It is a pleasure to thank Nick Whyborn for the careful and critical reading of the manuscript and Drs. Vladimir Usov, Sean Dougherty, Tony Moffat and Sergey Marchenko for stimulating discussions and correspondence. We thank the referee, Dr. R. White, for his constructive comments. Financial support for one of us (DYASG) from the Rotary Foundation, the University of Utrecht, and the Leids Kerkhoven-Bosscha Fonds is gratefully acknowledged. This research has made use of the SIMBAD data-base, operated at the CDS, Strasbourg, France.

References

Baars J.W.M., Genzel R., Pauliny-Toth I.I.K., Witzel A., 1977, A&A 61, 99
Bell A.R. 1978, MNRAS **182**, 147
Bos A., Raimond E., Someren Greve H.W., 1981, A&A 98, 251
Bregman J.D. 1993, in: O.M. Kolkman (ed), The Westerbork Synthesis Radio Telescope User Documentation, p. III-8-5
Conti P.S., 1988, in: P.S. Conti, A.B. Underhill (eds.), O Stars and Wolf-Rayet Stars, NASA SP-497, p. 61 (Table 1-29).
Dhillon V.S., Privett G.J., 1997, Starlink User Note 167.5.
Dougherty S.M., Williams P.M. 1999, WR146 – Observing the OB-type companion. In: van der Hucht K.A., Koenigsberger G., Eenens P.R.J.(eds.) Proc. IAU Symp. 193, Wolf-Rayet Phenomena in Massive Stars and Starburst Galaxies. ASP, San Francisco, p. 346
Dougherty S.M., Williams P.M., van der Hucht K.A., Bode M.F., Davis R.J., 1996, MNRAS 280, 963
Dougherty S.M., Williams P.M., Pollaco D.L. 2000, MNRAS (in press)
Eenens P.R.J., Williams P.M., 1994, 269, 1082
Eichler D., Usov V.V., 1993, ApJ 402, 271
Felli M., Massi M., 1991, VLBI observations of WR stars. In: van der Hucht K.A., Hidayat B. (eds.) Proc. IAU Symp. 143, Wolf-Rayet Stars and Interrelations with Other Massive Stars in Galaxies, Kluwer, Dordrecht, p. 87
Feast M.W., Whitelock P.A., 1997, MNRAS 291, 683
Helfand D.J., Schnee S., Becker R.H., White R.L., McMahon R.G., 1999, AJ 117, 1568
Horne J.H., Baliunas S.L., 1986, ApJ 302, 757
Jardine M.M., Allen H.R., Pollock A.M.T., 1996, A&A 314, 594
Koesterke L., Hamann W.-R., 1995, A&A 299, 503
Leitherer C., Robert C., 1991, ApJ 377, 629
Lépine S., Moffat A.F.J., 1999, ApJ 514, 909
Mezger P.G., Henderson A.P., 1967, ApJ 147, 471.
Moffat A.F.J. 1996, Asymmetries and inhomogeneities in Wolf-Rayet winds. In: Vreux J.-M., et al. (eds.), Proc. 33^{rd} Liège Int. Astroph. Coll,. Wolf-Rayet Stars in the Framework of Stellar Evolution, Univ. of Liège, Liège, p.199
Niemela V.S., Shara M.M., Wallace D.J., Zurek D.R., Moffat A.F.J., 1998, AJ 115, 2047
Noordam J.E. (ed.), 1994, NEWSTAR Cookbook
Pollock A.M.T., 1987, ApJ 320, 283
O'Sullivan J.D., 1984, in: 'Indirect Imaging', Cambridge University Press 299, 597
Pacholczyk A.G., 1970, Radio Astrophysics, Freeman, San Francisco
Press W.H., Teukolsky S.A., Vetterling W.T., Flannery B.P., 1992, Numerical Recipes 2nd ed., p. 569
Setia Gunawan D.Y.A., van der Hucht K.A., Stickland D.J., et al., 1995a, IUE monitoring of WR 140 (WC6+O4-5). In: van der Hucht K.A., Williams P.M. (eds.), Proc. IAU Symp. 163, Wolf-Rayet Stars: Binaries, Colliding Winds, Evolution, Kluwer, Dordrecht, p. 466.
Setia Gunawan D.Y.A., van der Hucht K.A., Stickland D.J., et al.m 1995b, An ultraviolet radial velocity orbit for WR 140 (WC6+O4-5). In: van der Hucht K.A., Williams P.M. (eds.), Proc. IAU Symp. 163, Wolf-Rayet Stars: Binaries, Colliding Winds, Evolution, Kluwer, Dordrecht, p. 508

Setia Gunawan D.Y.A., van der Hucht K.A., de Bruyn A.G., Williams P.M., 1996, The erratic 21 cm light-surve of WR 146 (HM19-3, WC6+OB). In: Vreux J.-M., et al. (eds.), Proc. 33rd Liège Int. Astroph. Coll,. Wolf-Rayet Stars in the Framework of Stellar Evolution, Univ. of Liège, Liège, p. 327

Setia Gunawan D.Y.A., de Bruyn A.G., van der Hucht K.A., Williams P.M., 1999, Radio light-curve for WR146 (HM19-3, WC6+OB), a colliding wind binary. In: van der Hucht K.A., Koenigsberger G., Eenens P.R.J. (eds.) Proc. IAU Symp. 193, Wolf-Rayet Phenomena in Massive Stars and Starburst Galaxies. ASP, San Francisco, p. 390

Smith L.F., Shara M.M., Moffat A.F.J., 1990, ApJ 358, 229

Smith L.F., Maeder A., 1989, A&A 211, 71

Taylor A.R., Goss W.M., Coleman P.H., van Leeuwen J., Wallace B.J., 1996, ApJS 107, 239

Usov V.V., 1992, ApJ 389, 635

van der Hucht K.A., 1992, A&AR 4, 123

van der Hucht K.A., Williams P.M., Spoelstra T.A.Th., de Bruyn A.G., 1992, Non-thermal radio observation of Wolf-Rayet stars: A case for long-period binaries. In: Drissen L., Leitherer C., Nota A. (eds.), Proc. STScI Workshop, Non-isotropic and Variable Outflows from Stars, PASPC 22, p. 253

van der Hucht K.A., Williams P.M., Spoelstra T.A.Th., Swaanenvelt J.P., 1995, Radio monitoring of the non-thermal Wolf-Rayet objects WR125, WR146 and WR147. In: van der Hucht K.A., Williams P.M. (eds.), Proc. IAU Symp. 163, Wolf-Rayet Stars: Binaries, Colliding Winds, Evolution, Kluwer, Dordrecht, p. 559

Weber E.J., Davies L. Jr., 1967, ApJ 148, 217

White R.L., Becker R.H., 1995, ApJ 451, 352.

White R.L., Chen W., 1995, Theory and observations of non-thermal phenomena in hot massive binaries. In: van der Hucht K.A., Williams P.M. (eds.), Proc. IAU Symp. 163, Wolf-Rayet Stars: Binaries, Colliding Winds, Evolution, Kluwer, Dordrecht, p. 438

Williams P.J.S. 1963, Nat 200, 56

Williams P.M., van der Hucht K.A., Pollock A.M.T., et al., 1990, MNRAS 243, 662

Williams P.M., van der Hucht K.A., Spoelstra T.A.Th., 1994, A&A 291, 805

Williams P.M., 1996, Radio emission from Wolf-Rayet and OB stellar winds. In: Taylor A.R., Paredes J.M. (eds.), Radio Emission from the Stars and the Sun, PASPC 93, 15.

Willis A.J.W., Dessart L., Crowther P.A., et al., 1997, MNRAS 290, 371

Wright A.E., Barlow M.J., 1975, MNRAS 170, 41